Journal of Photochemistry and Photobiology A: Chemistry 210 (2010) 100–107

Contents lists available at ScienceDirect

Journal of Photochemistry and Photobiology A: Chemistry

journal homepage: www.elsevier.com/locate/jphotochem

The theoretical trajectory for the chloride-ion-induced generation of singlet oxygen in the decomposition of dimethyldioxirane

Mikhail Yu. Ovchinnikov[a,*], Sergey L. Khursan[a], Dmitri V. Kazakov[a], Waldemar Adam[b,c]

[a] Institute of Organic Chemistry, Ufa Scientific Centre of the RAS, 71 Prospect Oktyabrya, 450054 Ufa, Russia
[b] Institut für Organische Chemie der Universität Würzburg, Am Hubland, D-97074 Würzburg, Germany
[c] Department of Chemistry, Facundo Bueso 110, University of Puerto Rico, Rio Piedras, PR 00931, USA

ARTICLE INFO

Article history:
Received 26 November 2009
Received in revised form 17 January 2010
Accepted 20 January 2010
Available online 1 February 2010

Keywords:
Chemiluminescence
Singlet oxygen
Cyclic peroxides
Reaction mechanism
Nucleophilic substitution
Catalysis

ABSTRACT

The mechanism of the catalytic chloride-ion-induced decomposition of dimethyldioxirane has been investigated from a theoretical point of view. The geometrical parameters and harmonic vibrational frequencies of the detected stationary points were calculated at the MP2/6-31+G(d) level of theory, the energies of all the stationary points were refined by means of the MP4(SDTQ)/6-31+G(d) approximation. It was found that the chloride ion forms complexes with acetone and dioxirane, the latter transforms to the anionic intermediate 2-chlorooxy-2-hydroxy propane alcoholate (**5b**) or ClO–C(CH_3)$_2$–O$^-$. Electrostatic forces stabilize these complexes, supported by the similar reaction enthalpies ($\Delta_r H°_{298.15\,K}$) and ion–dipole interaction energy (E). Our results reveal that the chloride-ion-induced decomposition of the peroxide is a four-step process in which the ClO–C(CH_3)$_2$–O$^-$ anion **5b** serves as a chain carrier in contrast to the earlier postulated hypochlorite ion. The critical step for the production of singlet oxygen is the strongly exothermic decomposition of the intermediate by its reaction with dimethyldioxirane. This chemiluminescent process takes place on the singlet potential energy surface (PES), for which spin conservation obliges the generation of electronically excited singlet oxygen. The present results require revision of the previously published mechanism.

1. Introduction

Singlet-oxygen ($^1O_2$) chemistry has been an attractive topic of intensive research over the years, in view of wide applications of $^1O_2$ in organic synthesis, its prominent environmental and biomedical significance, as well as its important role in chemiluminescence [1–11]. Peroxide reactions are the major chemical source of singlet oxygen. In particular, numerous systems based on hydrogen peroxide, endoperoxides, peroxy acids, trioxides, etc., have been reported to produce $^1O_2$ in high efficiency [5].

Recently, a new efficient way of singlet-oxygen generation has been reported, namely the catalytic decomposition of dioxiranes [12–15] by anionic nucleophiles, i.e. Cl^-, Br^-, I^-, t-BuO$^-$, O_2^- and OH^- [16,17]. Rather high yields of $^1O_2$ have been recorded in this peroxide system, e.g., ca. 100% for the reaction of dimethyldioxirane with chloride ion [17].

The mechanism in Scheme 1 was proposed [16,17] to account for the generation of $^1O_2$, which engages the nucleophilic attack of the hypochlorite ion on the dioxirane peroxide bond with formation of the intermediary peroxide anion **A**. Subsequent heterolytic cleavage of the latter into singlet oxygen and ketone releases the chloride ion, which is then again oxidized by another dioxirane molecule to complete the catalytic cycle.

Herein we report our theoretical study on the chloride-ion-induced catalytic decomposition of dioxiranes, which requires revision of the postulated mechanism in Scheme 1 in regard to the validity of structure **A** as intervening intermediate. As model case, we have chosen the parent dioxirane **1a**, the computations have been extended to the experimentally relevant dimethyl derivative **1b**. For the latter, our present high-level computations reveal a much more complex mechanistic scenario, in which the more likely precursor to the electronically excited singlet oxygen is the intermediate **11b** in Scheme 3 rather than the previously published [17] intermediate **A** in Scheme 1.

2. Experimental

Intensive testing of the potential energy surface (PES) for the reaction [including relaxed scan and intrinsic reaction coordinate (IRC) calculations] was carried out by various quantum-chemical methods. For all compounds, except the oxygen molecule, closed-shell restricted wave functions were employed. The Basis Set Superposition Error (BSSE) was assessed by Counterpoise (CP) correction. The energy parameters of the chloride-induced decom-

* Corresponding author. Tel.: +7 347 2356111; fax: +7 347 2356066.
E-mail address: chemlum@ufanet.ru (M.Yu. Ovchinnikov).

1010-6030/$ – see front matter © 2010 Elsevier B.V. All rights reserved.
doi:10.1016/j.jphotochem.2010.01.011

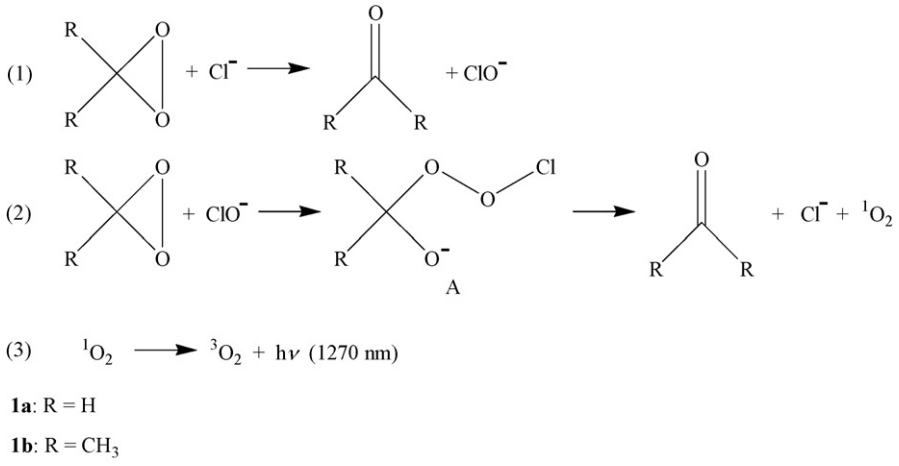

Scheme 1. Proposed mechanism for the generation of singlet oxygen in the catalytic decomposition of dioxiranes by the nucleophilic attack of the chloride ion.

Table 1
Computed distances (r_{ClO}) between the chlorine atom and the reacting oxygen atom in complex **2a**, transition state **3a**$^{\neq}$, and intermediate **4a** (see second, third and fourth stationary points in Fig. 1), and computed reaction enthalpies ($\Delta_r H^{\circ}_{298.15\,K}$) for the parent dioxirane **1a**, nucleophilically attacked by the chloride ion (Scheme 2).[a]

Basis set (MP2)	r_{ClO} (**2a**) (Å)	r_{ClO} (**3a**$^{\neq}$) (Å)	r_{ClO} (**4a**) (Å)	$\Delta_r H^{\circ}_{298.15\,K}$ (step 1) (kcal mol^{-1})	$\Delta_r H^{\neq}_{298.15\,K}$ (step 2) (kcal mol^{-1})	$\Delta_r H^{\circ}_{298\,K}$ (step 2) (kcal mol^{-1})
6-31+G(d)	4.528	2.391	1.721	−11.9	7.1	−2.0
6-311+G(d)	4.521	2.398	1.722	−11.5	7.4	−0.7
6-311+G(d,p)	4.510	2.406	1.723	−11.4	7.0	−1.7
6-311+G(2d,p)	4.531	2.378	1.711	−12.0	6.8	−2.1
6-311+G(3df,2p)	4.494	2.325	1.675	−12.4	7.7	−4.2
Method (6-31+G(d))						
MP4(SDTQ)//MP2	4.528	2.391	1.721	−11.9	4.2	−3.2
MP4(SDTQ)//MP4(SDQ)	4.535	2.316	1.734	−11.9	2.0	−3.5
CCSD(T)//CCD	4.543	2.186	1.721	−12.0	3.4	−2.2
QCISD(T)//QCISD	4.538	2.338	1.743	−13.7	4.1	−2.6

[a] Computed with the MP2 quantum-chemical method and various basis sets; several additional quantum-chemical methods were employed for the 6-31+G(d) basis set.

position for the parent dioxirane **1a** and its dimethyl derivative **1b** were obtained at 298.15 K. The transition states are labeled by '$\neq$', all other not coded ones correspond to equilibrium structures.

2.1. Quantum-chemical methods

The appropriate quantum-chemical method for the parent dioxirane **1a**, the model case, was chosen by considering the relevant geometrical parameters of the stationary points (stable compounds and transition states) and the optimal reaction heat ($\Delta_r H^{\circ}_{298.15\,K}$) for step 1 in Scheme 1. The salient results of our model computations are summarized in Table 1 and Fig. 1, the relevant mechanistic features of our calculations are displayed in Scheme 2.

Computations expose four stationary points, namely the reagents dioxirane **1a** and chloride ion, complex **2a**, transition state **3a**$^{\neq}$, and intermediate **4a**. The geometrical parameters of the structures **2a**, **3a**$^{\neq}$ and **4a**, calculated by means of the MP2/6-31+G(d) approximation, are shown in Fig. 1. Their key data are given in Table 1, whereas the bond distances of the parent dioxirane **1a** are presented in Table 2. The reaction enthalpies ($\Delta_r H^{\circ}_{298.15\,K}$) of the steps 1 and 2 (Scheme 2) are also collected in Table 1.

The choice of our computational method is subdivided into two parts, namely the *basis set* and *electron correlation*. As for the choice of the *basis set*, the MP2 quantum-chemical method was used. Our computed results reveal (Table 1) that the geometry and enthalpy parameters obtained with the 6-31+G(d) [19] basis set differ insignificantly from those provided by the more sophisticated basis sets. In regard to *electron correlation*, these calculations were carried out with the 6-31+G(d) basis set. As computational methods, we employed Coupled Clusters (CC), Configuration Interaction (CI), and Møller–Plesset Perturbation Theory [19], in conjunction with the 'frozen core' approximation.

Comparison of the experimental data with the calculations shows that all aforementioned methods give reasonable results (Table 2) in regard to the geometrical parameters for the parent dioxirane **1a**. The MP4(SDQ) method reproduces the structures of the stationary points quite well; however, poor convergence was noted during the self-consistent procedure for some structures with more than 14 atoms. Indeed, for the MPPT method it was reported that ... "*A convergent series in a DZP type basis, for example, may become divergent or oscillating in a large basis, especially if diffuse functions are present*"... [19]. The CCD method tends to underestimate key geometrical parameters of the transition state **3a**$^{\neq}$ (Table 1). No serious discrepancy was noted between the MP4(SDQ) and CCD versus the QCISD and MP2 level of theory; however, the MP2 method is characterized by low computation time and cost compared to the QCISD approximation. For this reason, the MP2 approxima-

Table 2
Experimental[a] and computed[b] bond distances of the parent dioxirane **1a**.

Bond distance (Å)	Experimental	MP2	MP4(SDQ)	CCD	QCISD
r(C–O)	1.388	1.403	1.397	1.393	1.397
r(C–H)	1.090	1.089	1.091	1.091	1.092
r(O–O)	1.516	1.538	1.526	1.509	1.525

[a] Experimental values taken from Ref. [18].
[b] Calculations were performed with 6-31+G(d) basis set.

Table 3
Ion–dipole interaction energy ($E_{ion-dipole}$)[a], reaction enthalpy ($\Delta_r H^\circ_{298.15\,K}$)[b], and CP correction for the complexes **2b**, **3b**, **7b**, and **8b**.[c].

Complex	$E_{ion-dipole}$ (kcal mol^{-1})	$\Delta_r H^\circ_{298.15\,K}$ (corrected) (kcal mol^{-1})	ΔE_{CP} (BSSE) (kcal mol^{-1})
2b	−15.1	−10.0	2.5
3b	−14.9	−10.9	2.7
7b	−15.1	−11.7	3.3
8b	−15.2	−12.7	3.5

[a] Calculated according to Eq. (1).
[b] Calculated with MP4(SDTQ)/6-31+G(d)//MP2/6-31+G(d).
[c] See structures in Fig. 2.

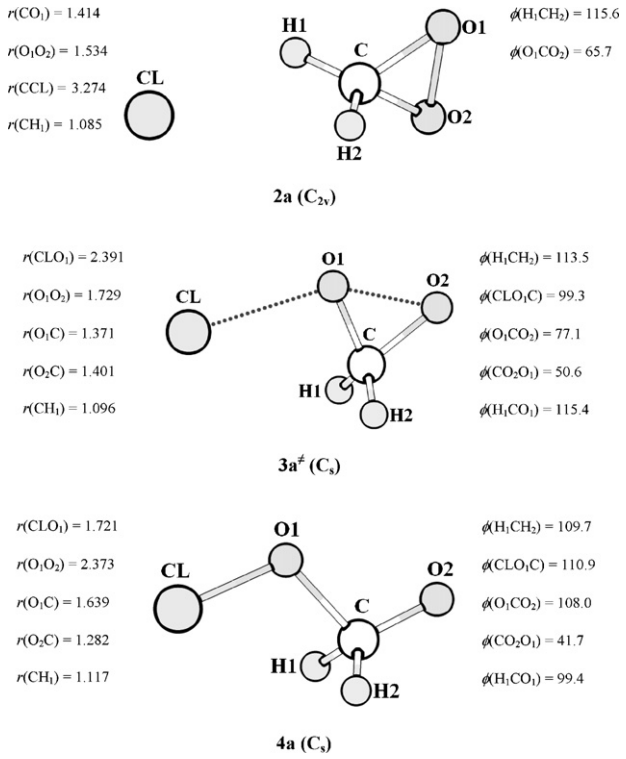

Fig. 1. Selected geometrical parameters of the MP2/6-31+G(d)-optimized structures for the second, third and fourth stationary points in the reaction of the parent dioxirane **1a** with the chloride ion (Scheme 2). Distances are given in Ångstroms, angles in degrees, and the appropriate Shehnflis notation is specified in parentheses for the symmetry in question.

tion was used as the optimal compromise. Consequently, the relaxed scan, the IRC calculations, as well as optimization and vibrational-frequency calculations were carried out with second-order Møller–Plesset Perturbation Theory for the chloride-ion reaction of the larger dioxirane **1b** with Pople's 6-31+G(d) basis set. Additionally, single-point energy calculations were performed with the MP4(SDTQ) method for more complete inclusion of electron correlation. All calculations employed Gaussian 03 Revision-D02 [20].

2.2. Ion–dipole interaction energy

For the calculation of the ion–dipole interaction energy (E) of the complexes, Eq. (1) was employed, in which ε is dielectric constant medium (we use $\varepsilon = 1$):

$$E = -\frac{1}{4\pi\varepsilon\varepsilon_0} \cdot \frac{q\mu\cos\Theta}{r^2}, \quad (1)$$

ε_0 is the dielectric constant for vacuum ($8.85418782 \times 10^{-12}$ F m^{-1}) [21], q is the ionic charge, μ is the dipole moment of the molecule in question, r is the distance between the ion and the center of dipole, and Θ is the angle between r and the dipole axis. The coordinates of the centers for the point charges used in the calculation of r and Θ have been computed by means of $x = \left(\sum_{i=1}^{N} x_i Z_i\right) / \sum_{i=1}^{N} Z_i$, in which i is index of the point charge, Z is the magnitude of the point charge, N is the total number of point charges, and x, y, and z are the Cartesian coordinates of the point charges in question. The point charges were estimated by means of the Natural Bond Orbital (NBO) analysis of the electron density at the MP4(SDTQ)/6-31+G(d) level of theory, the dipole moments were computed with the MP2/6-31G+(d) method.

3. Results

3.1. Molecular geometries

Analogous to the parent dioxirane **1a** as model case (Scheme 1), we have computed the reaction coordinate for the dimethyl-substituted dioxirane **1b** with chloride ion in acetone solution. Along this trajectory we found the complexes **2b**, **3b**, **7b** and **8b**, the transition states **4b**$^{\neq}$ and **9b**$^{\neq}$, the intermediates **5b**, its protonated form **6b** (in acidic media), **10b** and **11b**. The relevant geometrical parameters of these structures, as well as for dioxirane **1b**, are given in Fig. 2 [22]. The structures **4b**$^{\neq}$ and **9b**$^{\neq}$ are characterized by the imaginary vibrational frequencies 256 and 195 cm^{-1}. These frequencies meet the requirement of the nuclei being dis-

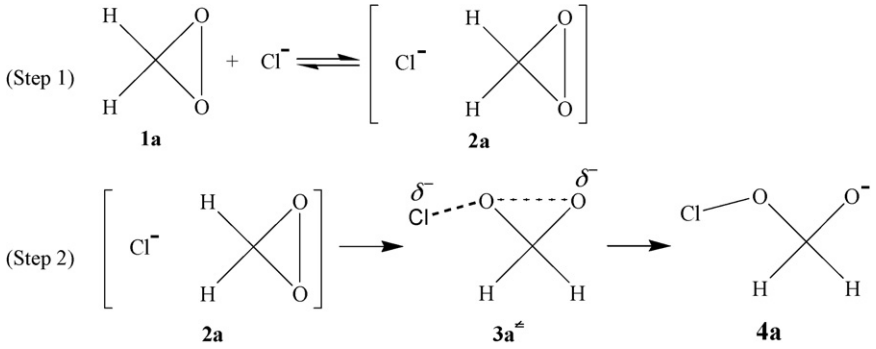

Scheme 2. Relevant mechanistic steps for the quantum-chemical computations of the model reaction of the parent dioxirane **1a** with the chloride ion.

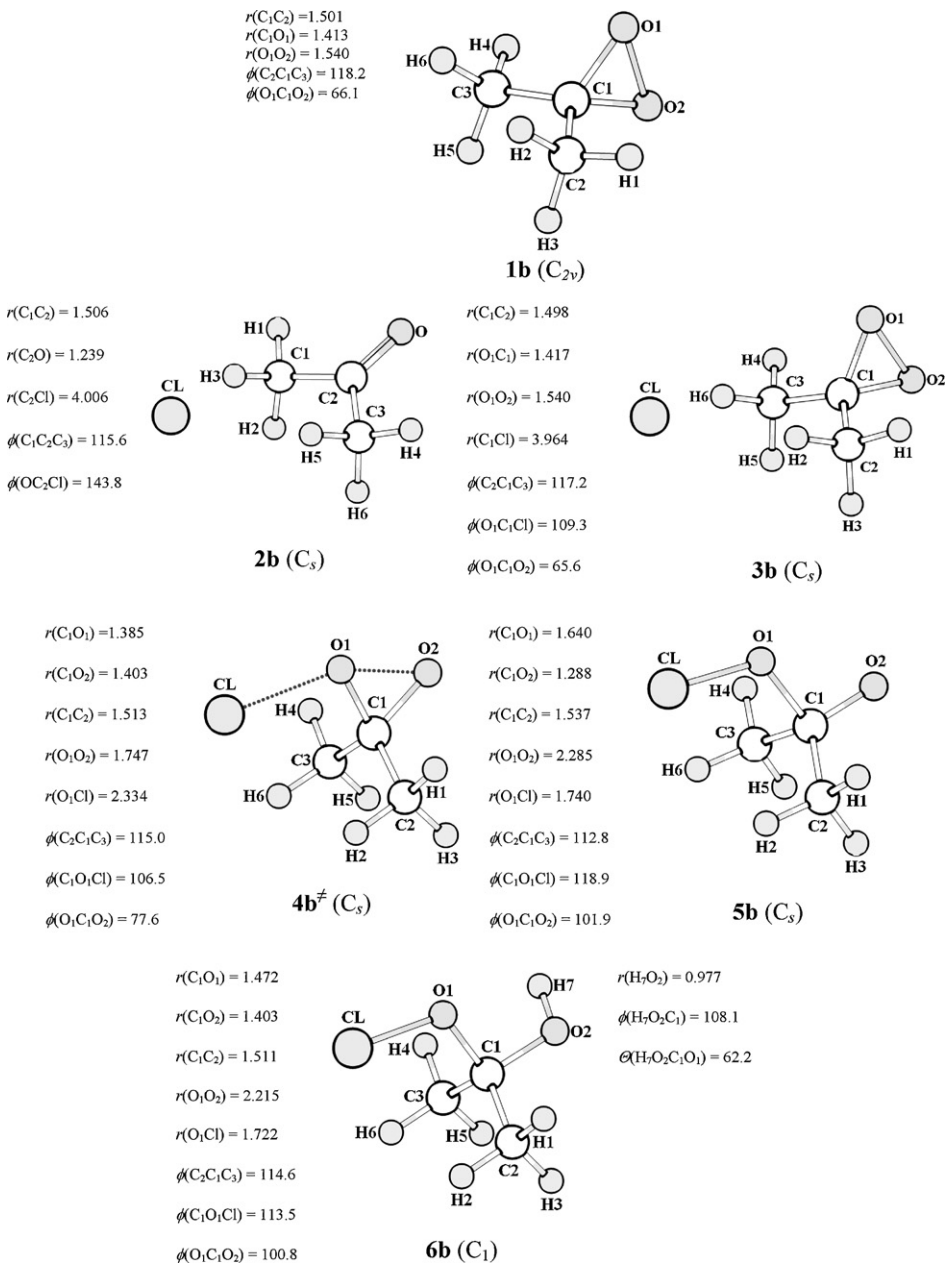

Fig. 2. Selected geometrical parameters of MP2/6-31+(d)-optimized structures for dioxirane **1b**, complexes **2b**, **3b**, **7b** and **8b**, intermediates **5b**, its protonated form **6b**, **10b** and **11b**, as well as transition states **4b**$^{\neq}$ and **9b**$^{\neq}$, localized on the singlet PES in the reaction of dioxirane **1b** with the chloride ion. The distances are given in Ångstroms, angles in degrees, and the symmetry in Shehnflis notation in parentheses.

placed along reaction coordinate. The latter coordinate and the IRC energy profiles (Figs. S1 and S2, see the Supporting Information section) validate the proposed transition states.

3.2. Ion–dipole interaction energies and reaction enthalpies of the revealed complexes

Since acetone and dioxiranes are polar molecules with dipole moments 3.61 and 3.55 Debye, it is reasonable to suppose that complexes **2b**, **3b**, **7b** and **8b** are stabilized by ion–dipole interaction. In addition, all structures are characterized by orientation of the dipole moment vector towards the ion (for example, see complex **3b** in Fig. 3), which also manifests the electrostatic nature of the bonding. Ion–dipole interaction energies ($E_{\text{ion–dipole}}$) and reaction heats ($\Delta_r H^{\circ}_{298.15\,K}$), the latter revised by CP corrections, of the complexes **2b**, **3b**, **7b** and **8b** are collected in Table 3 [23].

3.3. The fate of intermediate *5b*

The complex **3b**, found in our work, transforms through the opening of the dioxirane cycle to the intermediate **5b** (Fig. 2), a process of low activation barrier, namely $\Delta_r H^{\neq}_{298.15\,K} = 4.0$ and $\Delta_r G^{\neq}_{298.15\,K} = 5.4\,\text{kcal mol}^{-1}$ (Table 4, entry 2) [22]. The two trajectories shown in step 3 of Scheme 3[1] may be considered for further transformation of intermediate **5b**. In path [a] **5b** decomposes into acetone and ClO^-, the chain carrier postulated in Scheme 1 [17], whereas in path [b] the intermediate **5b** associates with another dioxirane **1b** molecule to form complex **8b**. The monomolecular decomposition of **5b**

[1] Atom indices in Scheme 3 correspond to those used in the computations shown in Fig. 2.

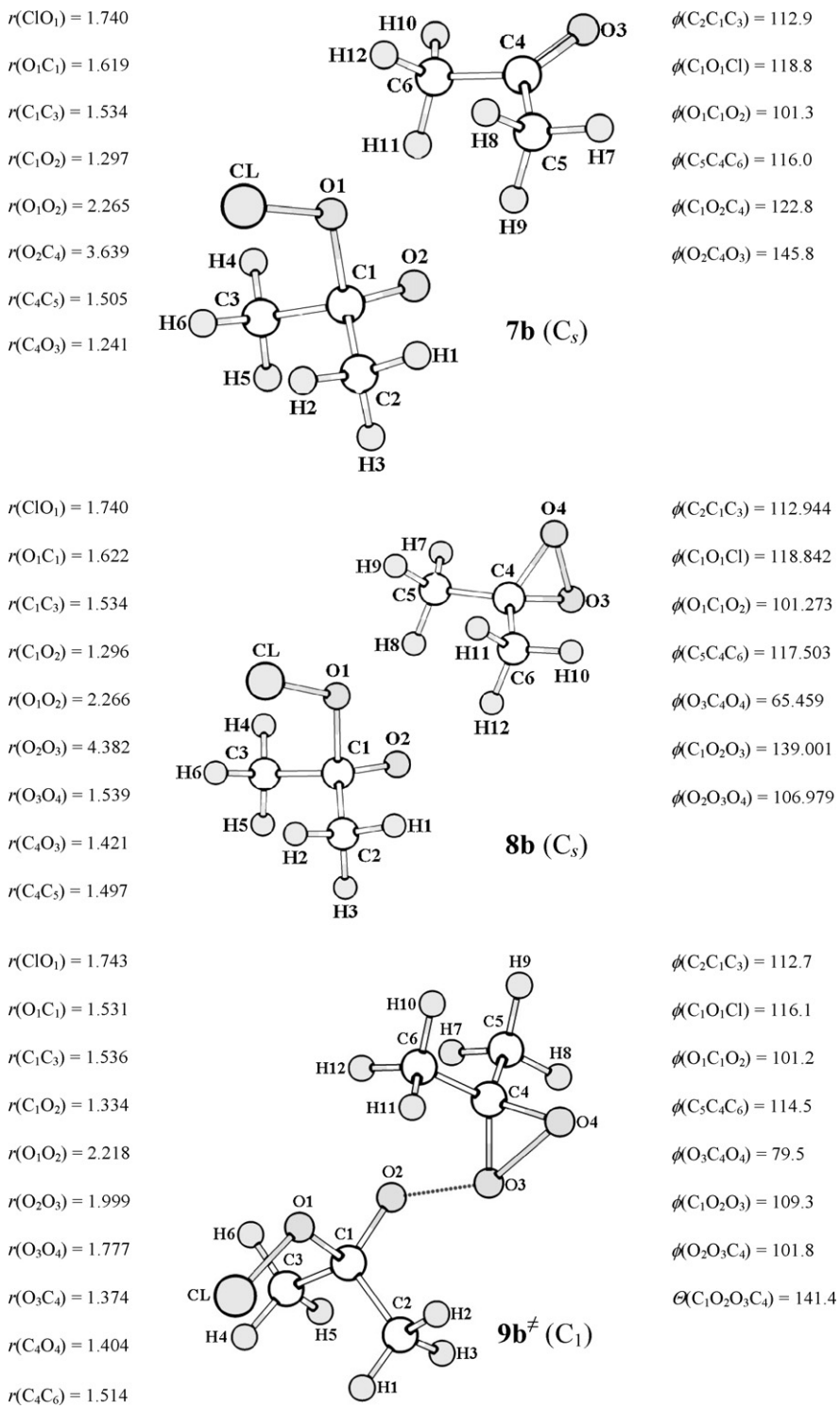

Fig. 2. *Continued*)

(path [a]) shown in step 3 was found to be endothermic by 15.4 kcal mol^{-1} with $\Delta G^{\circ} = 4.9$ kcal mol^{-1} [22]. By using the equilibrium equations $\Delta G^{\circ} = -RT \ln K_p$ and $K_c = K_p(RT)^{-\Delta\nu}$, we calculate for the equilibrium constant $K_c = 1 \times 10^{-5}$ mol/l and estimate for the ratio [**5b**]/[ClO^-] = K_c^{-1}·[CH_3COCH_3] as much as 1.4×10^6. Consequently, the formation of 'free' hypochlorite anion from intermediate **5b** (path [a]) in acetone solution is unlikely. Presumably, the bimolecular reaction (path [b]) of intermediate **5b** with dioxirane **1b** is favored to afford complex **8b**.

3.4. Singlet-oxygen formation and regeneration of the chloride-ion catalyst

The trajectory for the pivotal mechanistic event of singlet-oxygen release is mapped out in step (4) of Scheme 3. The complex **8b** transforms into the intermediate **10b** through the transition state **9b**$^{\neq}$, the latter is confirmed by IRC calculation starting from the **9b**$^{\neq}$ saddle point (see Fig. S2, Supporting Information section). In the critical step (path [a]), a new peroxide bond O_2–O_3 is formed at the expense of breaking the dioxirane peroxide bond O_3–O_4,

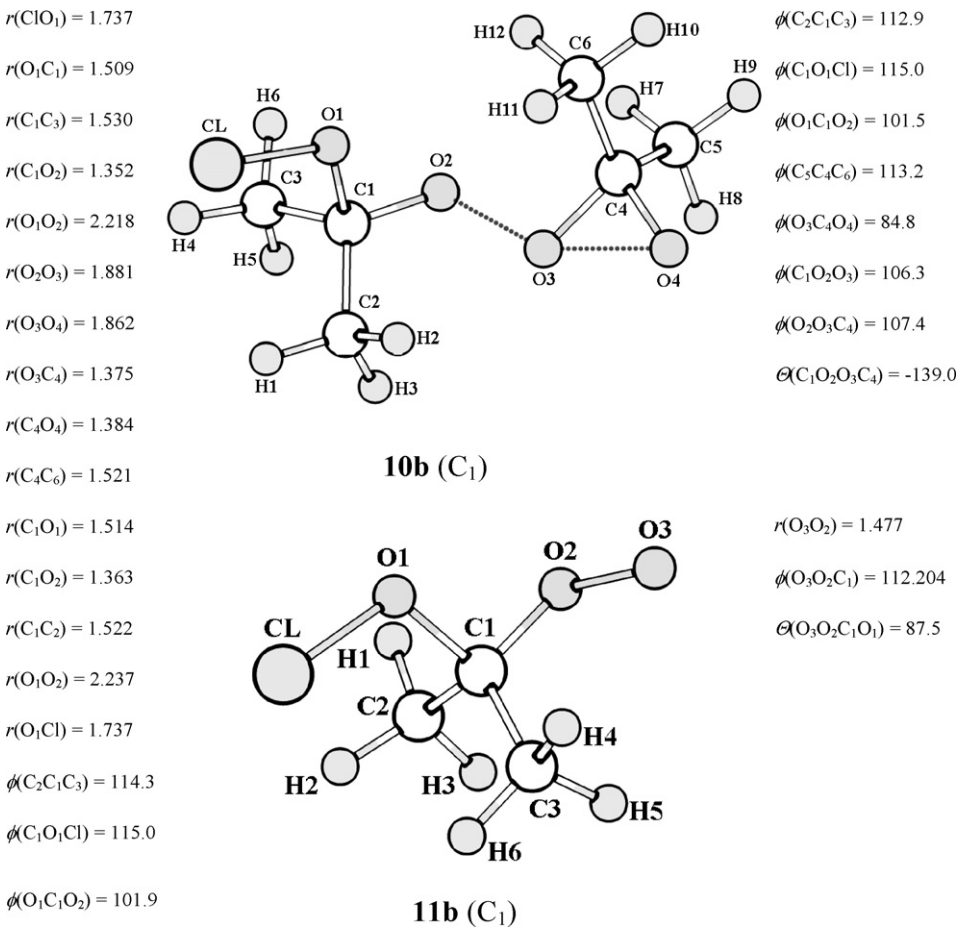

Fig. 2. *Continued*).

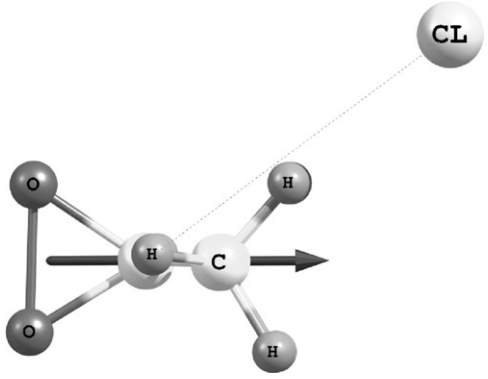

Fig. 3. Positional arrangement between the chloride ion and dioxirane **1b** in the complex **3b**, in which the arrow indicates the vector of the dipole moment.

to generate the intermediate **10b**. The alternative option of nucleophilic attack at the dioxirane carbon atom, usually the preferred route, may be excluded for energy reasons (Fig. S3 of the Supporting Information section). Subsequently, in path [b] intermediate **10b** ejects acetone to lead to the key structure **11b**, the precursor to singlet oxygen. The latter results from fragmentation of the intermediate **11b** along path [c], with concomitant regeneration of the acetone-solvated chloride ion, the catalytic species in this complex set of events. These mechanistic conclusions are backed up by our computations on the MP2/6-31+G(d) level of theory. Decomposition of intermediate **10b** should be very fast, since the MP4(SDTQ) PES of this process is rather flat, the energy difference in the various structures does not exceed 3 kcal mol^{-1}. The overall enthalpy change for the transformation of complex **8b** into the dioxygen, acetone and chloride ion (Table 4, entry 4) is highly exothermic. Therefore, enough energy is made available for the generation of dioxygen in its electronically excited state, $^1\Delta_g$.

Table 4
Computed energy parameters for the mechanistic steps in the catalytic production of singlet oxygen in the nucleophilic reaction between the chloride ion and dioxirane **1b**.[a].

Step	$\Delta_r H^\circ_{298.15\,K}$ (kcal mol^{-1})	$\Delta_r G^\circ_{298.15\,K}$ (kcal mol^{-1})	$\Delta_r H^{\neq}_{298.15\,K}$ (kcal mol^{-1})	$\Delta_r G^{\neq}_{298.15\,K}$ (kcal mol^{-1})
1[a]	−0.8	−0.1	–	–
2	1.4	2.6	4.0	5.4
3, path [b][a]	−1.3	1.6	–	–
4[a,b]	−42.3	−64.4	1.0	4.1

[a] Enthalpy and Gibbs free energy have been calculated by taking into account the solvation of the chloride ion and intermediate **5b** by acetone (structures **2b** and **7b** in Fig. 2).
[b] Enthalpy and Gibbs free energy of the overall reaction was calculated relative to the ground-state O_2 ($^3\Sigma_g^-$).

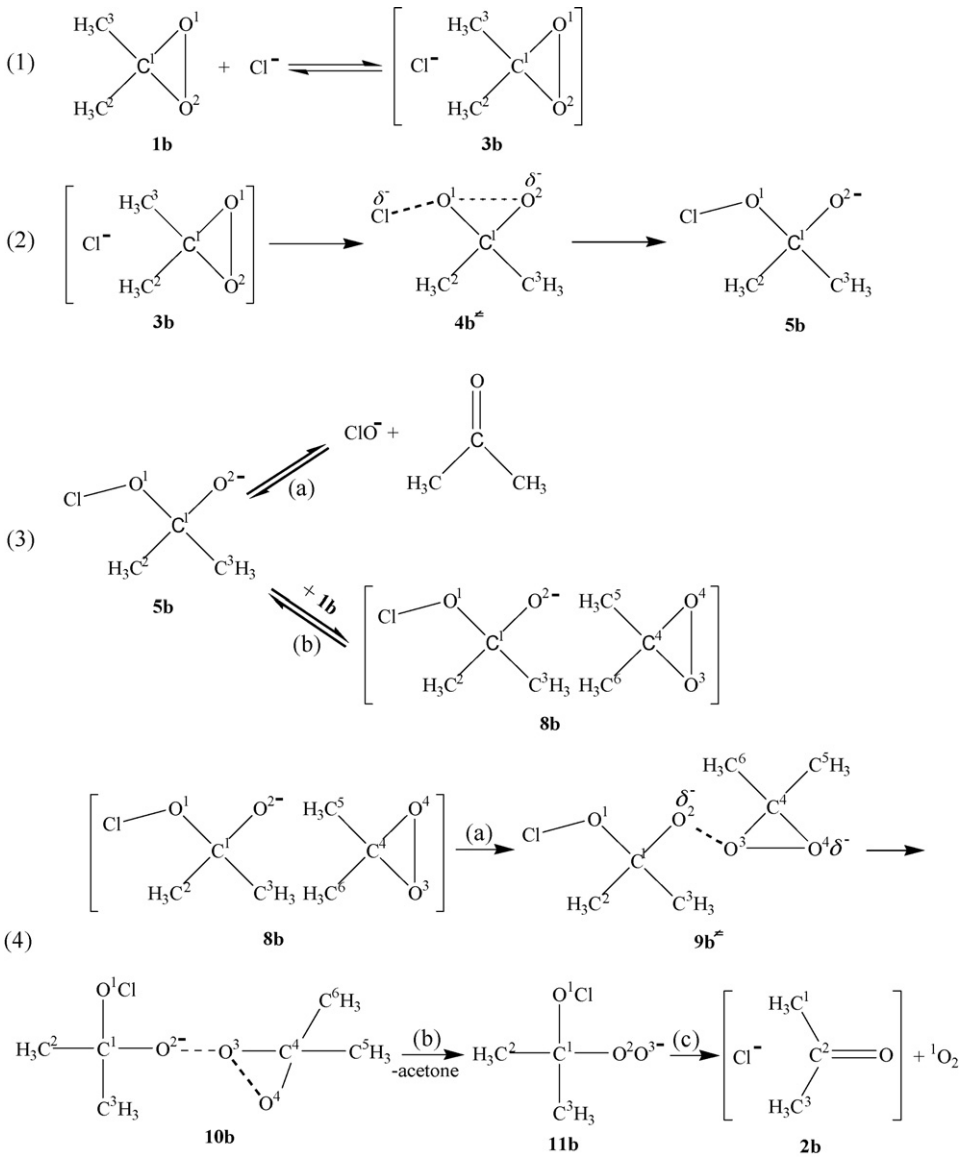

Scheme 3. Generation of the alcoholate **5b** intermediate, the mechanistic options for its transformation and relevant mechanistic steps for the production of singlet oxygen from complex **8b**.

4. Discussion

Our quantum-chemical study discloses that in the catalytic reaction of dioxirane **1b** with the chloride ion, the singlet oxygen is generated according to the sequence of steps exhibited in Scheme 3. The composite assembly of these four consecutively numbered steps provides the mechanistic panorama of this unusual chemiluminescent process. First let us address the three events in Scheme 3: in step (1), the complex **3b** is formed from the dioxirane **1b** and the chloride ion, the binding is characterized by ion–dipole interaction (Fig. 2). Notably, analogous to complex **3b**, also the complexes **2b**, **7b** and **8b** are held together by such ion–dipole interactions. Indeed, as may be seen from Table 3, the ion–dipole interaction energy correlates well with the reaction enthalpies of these complexes. In step (2), the intermediate **5b** results, in which the original dioxirane peroxide bond O_1–O_2 is totally broken. The C_1–O_2 bond length of 1.288 Å in the intermediate **5b** approaches that found in acetone, as attested by the C_2–O bond length of 1.239 Å in the acetone complex **2b** of Fig. 2. Earlier it was reported [17] that the chloride-ion-induced decomposition of dioxirane **1b** is significantly inhibited by the addition of carboxylic acids such as CH_3COOH or CF_3COOH. This fact may now be explained in terms of protonation at the negatively charged oxygen atom (the alkoxide-ion center O_2^-) in the intermediate **5b**, to afford the non-reactive species **6b** (Fig. 2). In step (3), the intermediate **5b** associates with another dioxirane **1b** molecule to result in complex **8b** rather than ejecting a hypochlorite ion.

The pathways a–c of step 4, the last event of Scheme 3, describe the important chemi-excitation process of generating the electronically excited singlet-oxygen product. In the first event, path [a], the complex **8b** transforms by way of transition state **9b**$^{\neq}$ to the intermediate **10b**. The latter eliminates acetone in path [b] to afford the intermediate **11b**, the precursor to $^1O_2$. Finally, fragmentation of **11b** in path [c] leads to singlet oxygen. Indeed, the PES of this crucial process is a singlet surface and, therefore, the spin-conservation rule dictates that the molecular oxygen is liberated electronically excited, namely in its $^1\Delta_g$ state. Since the decomposition of complex **8b** is by 42.3 kcal mol^{-1} exothermic (see Table 4), and the $^1\Delta_g$ state of singlet oxygen lies only 22.5 kcal mol^{-1} above the triplet ground state of molecular oxygen [1–10], more than enough energy is available to release electronically excited product.

Our present theoretical work on the chemi-excitation mechanism of singlet-oxygen ($^1O_2$) production in the catalytic

Cl^--induced decomposition of dioxirane **1b**, as exposed in the four steps of Scheme 3, mandates revision of the previously reported mechanism proposed in Scheme 1 [17]. The key feature of the two mechanisms is the structure of the immediate precursor to $^1O_2$: in Scheme 1, the intermediate **A** was postulated as the source of singlet oxygen, with the free hypochlorite ion as the chain-carrying species. In contrast, our present high-level computations, summarized in Scheme 3, substantiate that $^1O_2$ evolves from fragmentation of intermediate **11b**:

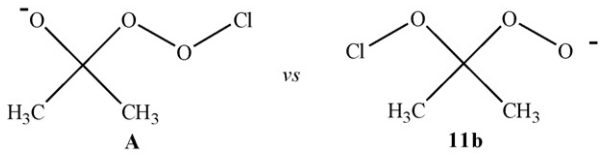

A **11b**

Indeed, we have definitively shown that no free hypochlorite ion is available in acetone solution and, thus, cannot serve as chain carrier in this catalytic process. The earlier intermediate **5b** in our mechanistic sequence, which eventually is transformed into intermediate **11b**, arrests all free hypochlorite ion in the acetone solution. Such adducts as intermediate **5b** were previously proposed for the reaction of the hypochlorite ion with formaldehyde [24] and with cyclobutanone [25] in aqueous solution. Moreover, our attempts to localize an equilibrium structure of the earlier proposed intermediate **A** (Scheme 1) both on the MP2 and QCISD level of theory were unsuccessful. The initially chosen geometry of **A** transforms in the course of the optimization to acetone, O_2, and Cl^-, which clearly implies that the intermediate **A** cannot exist as a stable species.

An additional significant finding of our computations, distinct from previous results, is the formation of various physically (ion–dipole interaction) bonded complexes. For example, the chloride ion and the anionic intermediate **5b** interact with acetone to form the reversible complexes **2b** and **7b**, which stabilize the intermediary catalytic species by specific solvation. Furthermore, Cl^- and **5b** interact with dioxirane **1b** to form the complexes **3b** and **8b**, whose subsequent unimolecular transformation leads eventually to singlet oxygen in the catalytic process of dioxirane **1b** decomposition.

5. Conclusion

The hyperenergetic dioxiranes [12,14,26,27] generate efficiently singlet oxygen in their chloride-ion-induced decomposition. This rare catalytic organic peroxide reaction is one of the most efficient chemiluminescent transformations for dioxiranes [5]. Our high-level computations reveal that this catalytic process involves a complex molecular trajectory, in which the formerly reported hypochlorite ion [17] is not the chain-carrying species. Instead of the previously postulated intermediate **A**, we show that the presently discovered intermediate **11b** is the immediate precursor to the electronically excited singlet-oxygen product.

Acknowledgements

The research in Ufa was supported by the Russian Foundation for Basic Research (Grant No. 09-03-00831-a), Grant of President of RF for support of young scientists (Grant No. MD-3852.2009.3), the Branch of Chemistry and Material Sciences of the RAS (No. 1-OKh), as well a WA thanks the Deutsche Forschungsgemeinschaft (DFG), Fonds der Chemischen Industrie, and the Alexander von Humboldt-Stiftung for many years of financial support, and the University of Puerto Rico, Rio Piedras Campus for generous hospitality.

Appendix A. Supplementary data

Supplementary data associated with this article can be found, in the online version, at doi:10.1016/j.jphotochem.2010.01.011.

References

[1] H.H. Wasserman, R.W. Murray, Organic Chemistry: Singlet Oxygen, vol. 40, Academic Press, New York, 1979.
[2] A.A. Frimer, Singlet Oxygen, CRC, Boca Raton, FL, 1985.
[3] W. Adam, T. Wirth, Hydroxy group directivity in the epoxidation of chiral allylic alcohols: control of diastereoselectivity through allylic strain and hydrogen bonding, Acc. Chem. Res. 32 (1999) 703–710.
[4] C. Schweitzer, R. Schmidt, Physical mechanisms of generation and deactivation of singlet oxygen, Chem. Rev. 103 (2003) 1685–1758.
[5] W. Adam, D.V. Kazakov, V.P. Kazakov, Singlet-oxygen chemiluminescence in peroxide reactions, Chem. Rev. 105 (2005) 3371–3387.
[6] J. Cadet, J.-L. Ravanat, G.R. Martinez, M.H.G. Medeiros, P. Di Mascio, Singlet oxygen oxidation of isolated and cellular DNA: product formation and mechanistic insights, Photochem. Photobiol. 82 (2006) 1219–1225.
[7] E. Skovsen, J.W. Snyder, P.R. Ogilby, Two-photon singlet oxygen microscopy: the challenges of working with single cells, Photochem. Photobiol. 82 (2006) 1187–1197.
[8] R. Schmidt, Photosensitized generation of singlet oxygen, Photochem. Photobiol. 82 (2006) 1161–1177.
[9] A.A. Krasnovsky Jr., Photoactivation of molecular oxygen. History of development and the modern status of research, Biochemistry (Moscow) 72 (2007) 1065–1080.
[10] B.F. Minaev, Electronic mechanisms of molecular oxygen activation, Russ. Chem. Rev. 76 (2007) 989–1011.
[11] D.V. Kazakov, V.P. Kazakov, G.Y. Maistrenko, D.V. Mal'zev, R. Schmidt, On the effect of 1,4-diazabicyclo[2. 2. 2]octane on the singlet-oxygen dimol emission: chemical generation of $(^1O_2)_2$ in peroxide reactions, J. Phys. Chem. A 111 (2007) 4267–4273.
[12] W. Adam, R. Curci, J.O. Edwards, Dioxiranes: a new class of powerful oxidants, Acc. Chem. Res. 22 (1989) 205–211.
[13] R.W. Murray, Chemistry of dioxiranes. 12. Dioxiranes, Chem. Rev. 89 (1989) 1187–1201.
[14] V.P. Kazakov, A.I. Voloshin, D.V. Kazakov, Dioxiranes: from oxidative transformations to chemiluminescence, Russ. Chem. Rev. 68 (1999) 253–286.
[15] W. Adam, C.R. Saha-Müller, C.-G. Zhao, Dioxirane epoxidation of alkenes, Org. React. 61 (2002) 219–516.
[16] V. Nagel, F. Duschek, W. Kiefer, F. Görth, D. Golsch, W. Adam, M. Ferrer, A. Messeguer, Detection of singlet oxygen during several organic reactions by chemiluminescence spectroscopy, Asian J. Spectrosc. 2 (1998) 35–43.
[17] W. Adam, D.V. Kazakov, V.P. Kazakov, W. Kiefer, R.R. Latypova, S. Schlücker, Singlet-oxygen generation in the catalytic reaction of dioxiranes with nucleophilic anions, Photochem. Photobiol. Sci. 3 (2004) 182–188.
[18] R.D. Suenram, F.J. Lovas, Dioxirane. Its synthesis, microwave spectrum, structure, and dipole moment, J. Am. Chem. Soc. 100 (1978) 5117–5122.
[19] F. Jensen, Introduction to Computational Chemistry, John Wiley & Sons, Chichester/New York/Weinheim/Brisbane/Singapore/Toronto, 1999.
[20] M.J. Frisch, G.W. Trucks, H.B. Schlegel, G.E. Scuseria, M.A. Robb, J.R. Cheeseman, V.G. Zakrzewski, J.A. Montgomery Jr., R.E. Stratmann, J.C. Burant, S. Dapprich, J.M. Millam, A.D. Daniels, K.N. Kudin, M.C. Strain, O. Farkas, J. Tomasi, V. Barone, M. Cossi, R. Cammi, B. Mennucci, C. Pomelli, C. Adamo, S. Clifford, J. Ochterski, G.A. Petersson, P.Y. Ayala, Q. Cui, K. Morokuma, D.K. Malick, A.D. Rabuck, K. Raghavachari, J.B. Foresman, J. Cioslowski, J.V. Ortiz, A.G. Baboul, B.B. Stefanov, G. Liu, A. Liashenko, P. Piskorz, I. Komaromi, R. Gomperts, R.L. Martin, D.J. Fox, T. Keith, M.A. Al-Laham, C.Y. Peng, A. Nanayakkara, M. Challacombe, P.M.W. Gill, B. Johnson, W. Chen, M.W. Wong, J.L. Andres, C. Gonzalez, M. Head-Gordon, E.S. Replogle, J.A. Pople, Gaussian 03 Revision-D02, Gaussian Inc., Pittsburgh, PA, 2004.
[21] N.M. Baron, A.M. Ponomareva, A.A. Ravdel', Z.N. Timofeeva, Kratkiy spravochnik fiziko-khimicheskih velichin (Short Hand-Book of the Physicochemical Values), tenth ed., Ivan Fedorov, Moscow, 2002.
[22] Total energies, the absolute values of the reaction enthalpy and Gibbs free energy of the structures presented in Fig. 2 are given in Table S1 of the Supporting Information section, as well as the Cartesian coordinates for the computations presented in Table S2.
[23] The Point Charges used for the calculation of ion–dipole interaction energy are available in the Supporting Information section.
[24] J.-S. Do, W.-C. Yeh, I-Ya. Chao, Kinetics of the oxidative degradation of formaldehyde with electrogenerated hypochlorite ion, Ind. Eng. Chem. Res. 36 (1997) 349–356.
[25] J.A. Horton, M.A. Laura, S.M. Kalbag, R.C. Petterson, Reaction of hypochlorous acid with ketones. Novel Baeyer-Villiger oxidation of cyclobutanone with hypochlorous acid, J. Org. Chem. 34 (1969) 3366–3368.
[26] W. Adam, R. Curci, Hyperenergetic molecules: dioxetanes and dioxiranes, Chim. Ind. (Milan) 63 (1981) 20–28.
[27] D.V. Kazakov, A.B. Barzilova, V.P. Kazakov, A novel chemiluminescence from the reaction of dioxiranes with alkanes. Proposed mechanism of oxygen-transfer chemiluminescence, Chem. Commun. (2001) 191–192.